

Supplementary Materials

Polar-group functionalized polyetherimide separator with accelerated Li-ion transport for stable lithium metal batteries

Yana Sun, Jinyun Zheng^{*}, Huajie Zhu, Mingrui Yang, Enhui Wang, Xiaoni Guo, Xiangming Feng^{*}, Weihua Chen

College of Chemistry, Zhengzhou University, Zhengzhou 450001, Henan, China.

***Correspondence to:** Dr. Jinyun Zheng, Dr. Xiangming Feng, College of Chemistry, Zhengzhou University, No. 100 Science Avenue, Zhengzhou 450001, Henan, China, E-mail: zhengjy@zzu.edu.cn; fengxm@zzu.edu.cn

Electrochemical measurement and cells assembly

The LiFePO₄ (LFP), Super P and poly (vinylidene fluoride) (PVDF) in the weight percentage of 80:10:10 were uniformly dispersed in N-methylpyrrolidone (NMP) to form a black slurry, and then was casted on Al foil. Then, LiFePO₄ cathodic sheet was obtained after drying at 60 °C for 8 h. Subsequently, 2025-type coin cells were assembled with anode of Li-metal and electrolyte (1 M LiPF₆ dissolved in EC:DMC:EMC=1:1:1 Vol%) in argon-filled glovebox (Mikrouna, Super) at room temperature. The LiFePO₄ cathodes were cut into 12 mm diameter discs with an area loading of 1.50–2.10 mg cm⁻². For the high loading LiFePO₄ cathodes, the area loading were 8.64–8.87 mg cm⁻². The size of LiFePO₄ cathode plate of the pouch cell was 5.5 cm × 4.3 cm, and the loading of active material was about 9.20 mg cm⁻². The LiFePO₄ based cells were evaluated by programmed Neware battery testing system (Shenzhen, China, MIHW-200-160CH and CT-4008) at 25 °C in voltage range of 2.8–4.0 V. In addition, LiCoO₂ (LCO) and LiNiCoAlO₂ (NCA) coin cells were also assembled and assessed in the same procedure. Differently, the potential window was changed to 3.0–4.5 V and 3.0–4.2 V, respectively. LiCoO₂ (LCO) and LiNiCoAlO₂ (NCA) cathodes were also prepared by same method. The area loading of LiCoO₂ and LiNiCoAlO₂ cathodes were 1.94–2.08 mg cm⁻² and 2.13–2.28 mg cm⁻², respectively. The performances of the cells at high temperatures of 60 °C were assembled with electrolyte of 0.5 M LiBOB in PC:DEC=3:7 Vol%. The electrochemical impedance spectroscopy (EIS) tests and Li⁺ ion transference number were measured by Li||Li symmetric cells. The Li||Cu cells were assembled to test the efficiency of lithium deposition and stripping with different separators in the voltage range of 0–1.0 V (vs. Li/Li⁺).

The contact angle tests of separators with electrolyte (1 M LiPF₆ dissolved in EC:DMC:EMC=1:1:1 Vol%) were examined with contact angle measurement analyzer (Dataphysics-OCA20). The morphologies of separators were examined with scanning electronic microscope (SEM, ZEISS Merlin Compact). The polar groups of

PEI and PEI-EDA were verified by fourier transform infrared spectroscopy (FT-IR, VECTOR 22). STA449F3 synchronous thermal analyzer (NETZSCH Instruments Co., Ltd.) was employed to investigate the thermal stability from 30 °C to 600 °C with a heating rate of 10 °C min⁻¹ under an argon atmosphere. The ion conductivity of electrolyte-saturated separator was detected with Electrochemical Impedance Spectroscopy (EIS, Solartron 1480E chemical workstation) in the range of 0.01 Hz–10⁵ Hz. And the cyclic voltammetry (CV) of PP, PEI and PEI-EDA separators were detected from 2.6–4.2 V at the 0.5 mV s⁻¹. The composition of the solid electrolyte interphase (SEI) films on Cu foils surface with different separators were measured by X-ray photoelectron spectroscopy (XPS) (AXIS Supra X). The interaction of PEI-EDA separator with the electrolyte was measured by NMR (AVANCE III HD600MHz). The cathode electrolyte interphase (CEI) films of LiFePO₄||Li cells with different separators were measured by transmission electron microscope (TEM) (Tecnai G2 F30). The gas production of Li||LFP cells with different separators were measured by on-line electrochemical mass spectroscopy (OLEMS) (AHPR-20-DEMS).

The porosity of separator was measured by the n-butanol immersion method. The dry separator was soaked in-butanol (≥99.7 %) for 24 h at room temperature, and the porosity was calculated using the following equation (1):

$$Porosity(\%) = \frac{m_3 - m_2}{V \times \rho} \times 100\%$$

where the m_2 and m_3 are the weight of the pristine and after absorbing n-butanol separator, respectively. V is the total volume of the separator, and ρ is the density of n-butanol.

The electrolyte uptake of the separator was calculated with the following Equation (2):

$$Electrolyte\ uptake(\%) = \frac{m_1 - m_0}{m_0} \times 100\%$$

where m_0 and m_1 are the weight of the pristine and the saturated in electrolyte for 2

hours separator, respectively.

To estimate ionic conductivity (σ) of the separators, the bulk resistance of the separator R_b was calculated initially by the Nyquist plot of the symmetric stainless steel cells (SS||SS). The electrochemical impedance spectroscopic measurements (EIS, Solartron 1480E) used to obtain Nyquist plot, which was tested at the open-circuit voltage (OCV) and applied AC voltage of 10 mV amplitude in the frequency range of 0.1 Hz to 100 KHz. The ionic conductivity was calculated using equation (3):

$$\sigma = \frac{d}{R_d \times S}$$

where d , R_d , and S are the thickness, the resistance and the area of stainless steel, respectively.

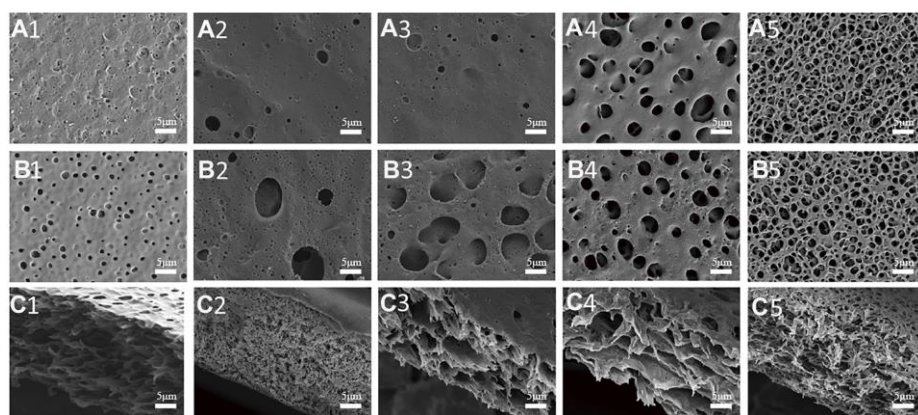
According to the Bruce-Vincent method, DC polarization measurements were conducted with a potential of $\Delta V=10$ mV for 2000 s in the Li||Li symmetric cells until the current reached a steady state. Li^+ ion transference number (t_{Li^+}) was calculated by the following Equation (4):

$$t_{\text{Li}^+} = \frac{I_s(\Delta V - I_0 R_0)}{I_0(\Delta V - I_s R_s)}$$

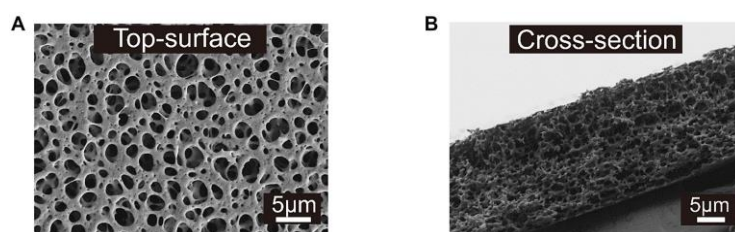
Where I_s and I_0 account for the steady-state current and the initial-state current. ΔV is the voltage pulse by DC polarization. R_s and R_0 refer to the steady-state interfacial resistance and the initial interfacial resistance.

The activation energy (E_a) was calculated based on the plot of ionic conductivity (σ) vs ($1/T$) from 25 °C to 65 °C according to Arrhenius Equation (5):

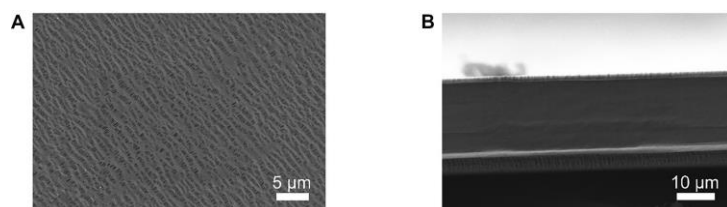
$$\sigma = A \exp\left(\frac{-E_a}{RT}\right)$$



Supplementary Figure 1. The SEM images of the upper surface, lower surface and cross-section of PEI membranes obtained with different pore forming agent contents.



Supplementary Figure 2. SEM morphology images of PEI separator: (A) top-surface, (B) cross-section.

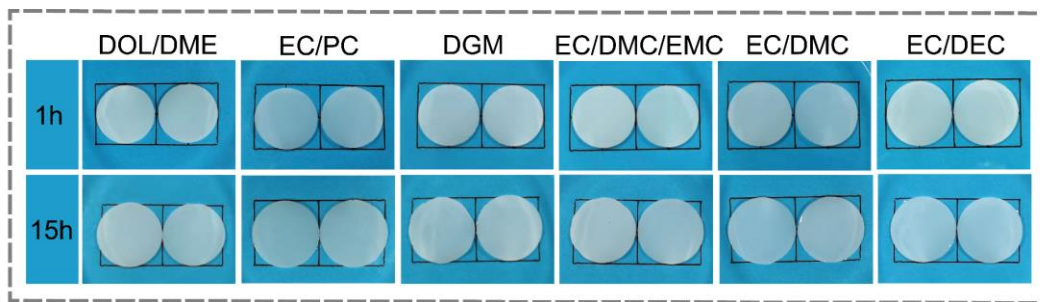


Supplementary Figure 3. SEM morphology images of PP separator: (A) top-surface, (B) cross-section.

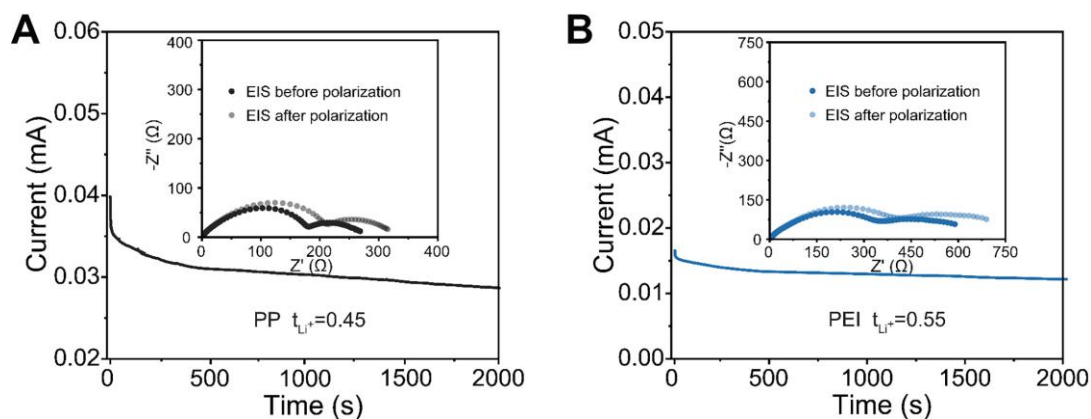


Supplementary Figure 4. Mechanical abuse tests for PEI-EDA separator.

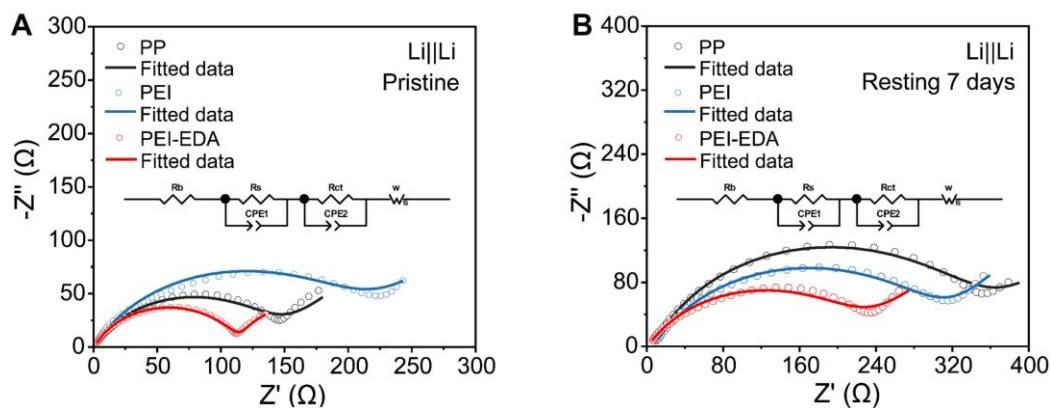
Supplementary Videos. The burning tests of three separators.



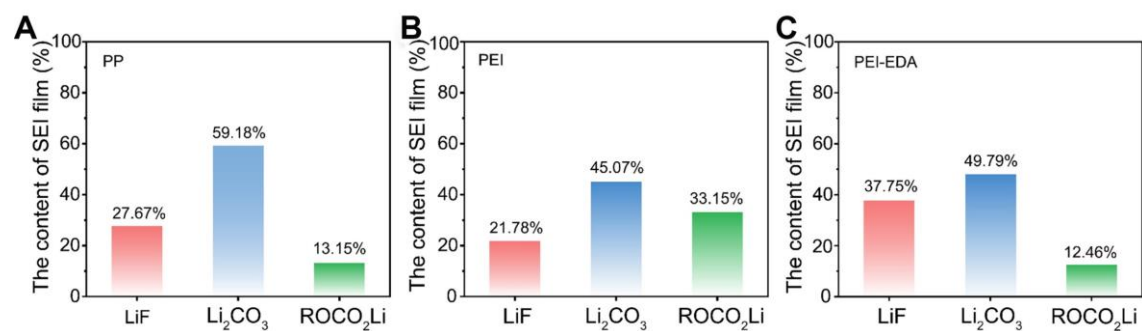
Supplementary Figure 5. Stability of PEI-EDA separator in different electrolyte solvent.



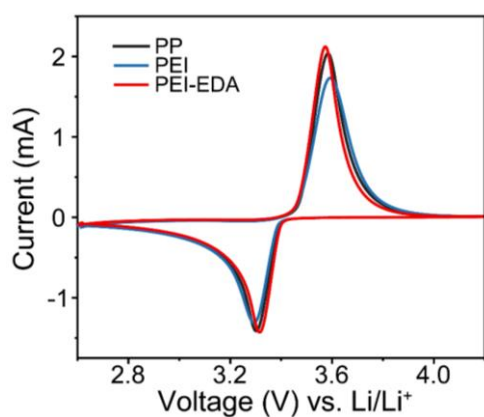
Supplementary Figure 6. Li^+ ion transference number (inset: Nyquist plots before and after polarization): (A) PP, (B) PEI.



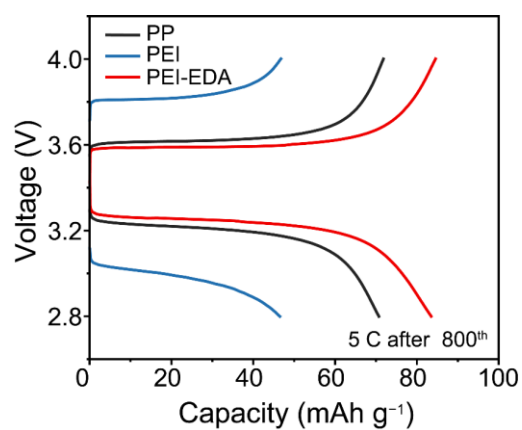
Supplementary Figure 7. EIS spectra of $\text{Li}||\text{Li}$ symmetric cells with different separators at different cycle times: (A) Pristine, (B) Resting 7 days.



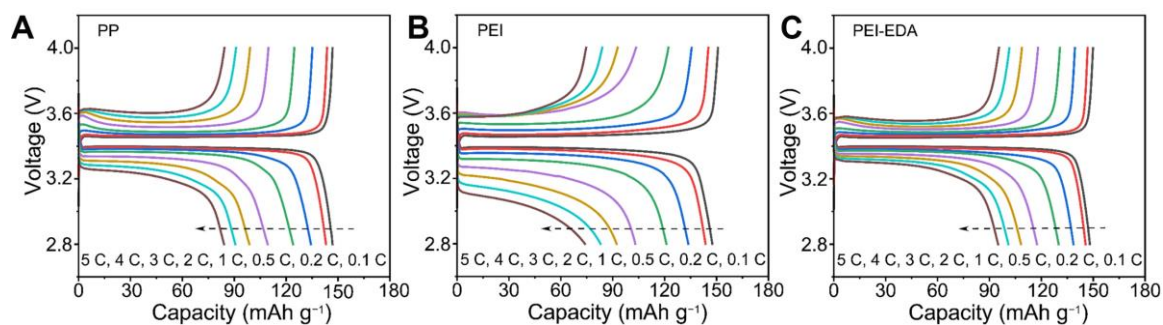
Supplementary Figure 8. The area ratio of surface SEI components in Li 1s assembled with different separators: (A) PP, (B) PEI, (C) PEI-EDA.



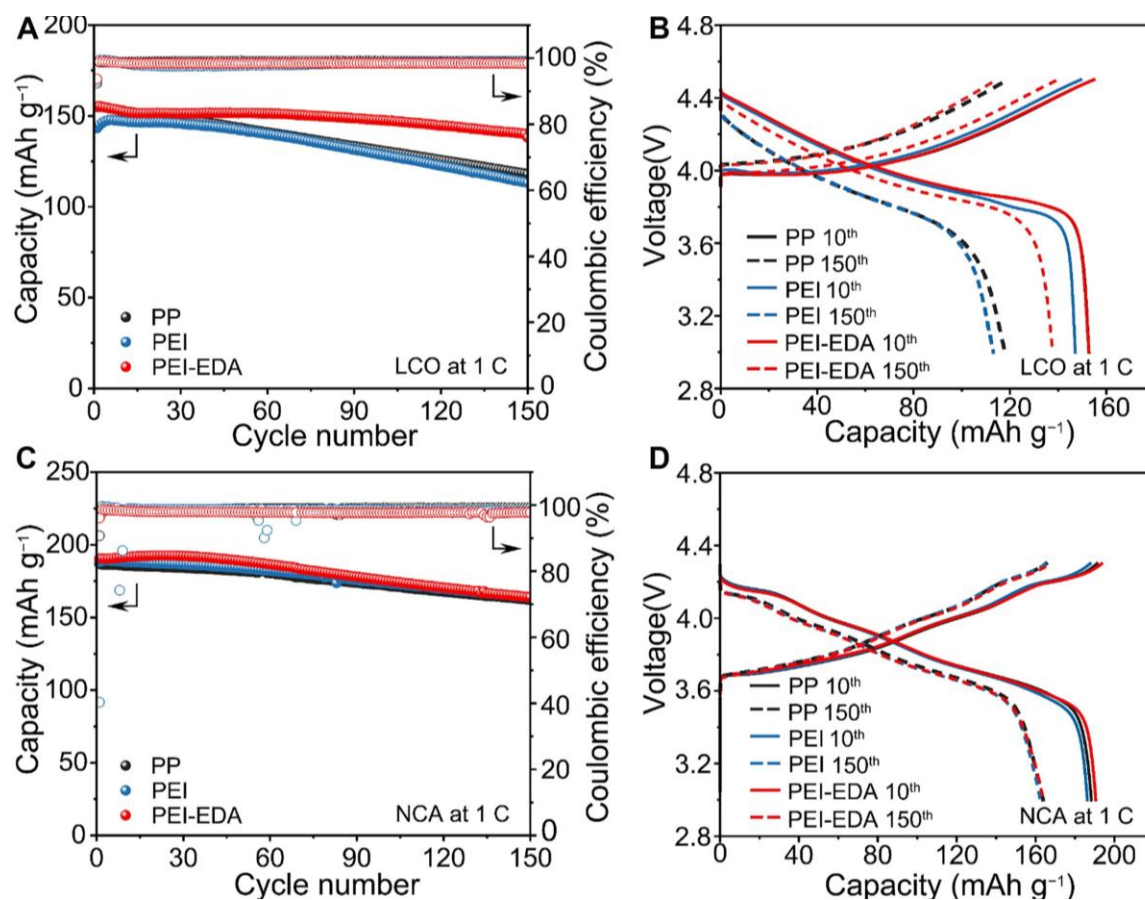
Supplementary Figure 9. CV curve at 0.5 mV s^{-1} with PP, PEI and PEI-EDA separator.



Supplementary Figure 10. Corresponding galvanostatic charge and discharge curves after 800 cycles at 5 C with PP, PEI and PEI-EDA separator.



Supplementary Figure 11. Corresponding galvanostatic charge and discharge curves at different rates with different separator: (A) PP, (B) PEI, (C) PEI-EDA.



Supplementary Figure 12. Electrochemical performance of Li||LCO cells with different at the current density of 1 C: (A) Cycling performance, (B) Corresponding galvanostatic charge and discharge curves after 10 and 100 cycles. Electrochemical performance of Li||NCA cells at the current density of 1 C: (C) Cycling performance, (D) Corresponding galvanostatic charge and discharge curves after 10 and 100 cycles.

Supplementary Table 1. Summary of impedance-fit data of Li||Li symmetric cells with different separators

	Pristine		Resting 7 days		After 50 cycles	
	$R_b[\Omega]$	$R_{int}[\Omega]$	$R_b[\Omega]$	$R_{int}[\Omega]$	$R_b[\Omega]$	$R_{int}[\Omega]$
PP	4.36	139.10	9.40	331.30	7.65	54.14
PEI	4.82	201.70	12.13	303.90	7.49	66.65
PEI-EDA	2.98	107.90	6.55	216.50	4.03	28.31

Supplementary Table 2. The electrochemistry performances compared with recent reports

Materials	Rate	Cathode Anod	Capacity Retention (%)	Refs.
DMS@PP	1 C	Li LFP	85.0% (after 1000 cycles)	Adv. Funct. Mater. 2023, 33, 2301586
EAA75	1 C	Li LFP	69% (after 200 cycles)	ACS Appl. Mater. Interfaces 2023, 15, 18333–18342
BA@ATP-14	1 C	Li LFP	91.38% (after 300 cycles)	Energy Storage Mater. 2022, 48, 123–132
LS	1 C	Li LFP	92.9% (after 500 cycles)	Adv. Mater. 2024, 36, 2311529
CNT@PDA/PVDF-HFP	5 C	Li LFP	87.35% (after 800 cycles)	Adv. Funct. Mater. 2024, 34, 2308929
ESM	5 C	Li LFP	94.7% (after 200 cycles)	Energy Storage Mater. 2018, 14, 258–266
P@AS	1 C	Li LFP	93.56% (after 300 cycles)	Small 2024, 2404470
PEI-EDA	5 C	Li LFP	92.3% (after 800 cycles)	This work